

Computational Design and Discovery of Nanomolar Inhibitors of I κ B Kinase β

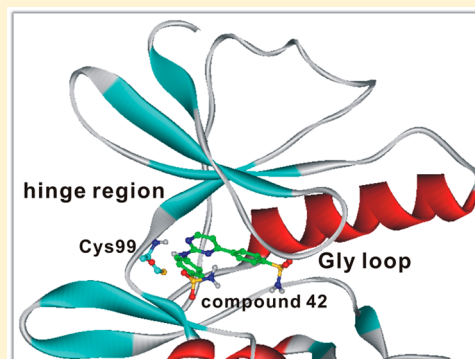
Hwangseo Park,^{*,†} Yongje Shin,[‡] Hyeonjeong Choe,[‡] and Sungwoo Hong^{*,‡}

[†]Department of Bioscience and Biotechnology, Sejong University, Seoul 143-747, Korea

[‡]Center for Catalytic Hydrocarbon Functionalization, Institute for Basic Science (IBS) and Department of Chemistry, Korea Advanced Institute of Science and Technology (KAIST), Daejeon, 305-701, Korea

S Supporting Information

ABSTRACT: I κ B kinase β (IKK β) is a useful target for the discovery of new medicines for cancer and inflammatory diseases. In this study, we aimed to identify new classes of potent IKK β inhibitors based on structure-based virtual screening, *de novo* design, and chemical synthesis. To increase the probability of finding actual inhibitors, we improved the scoring function for the estimation of the IKK β -inhibitor binding affinity by introducing proper solvation free energy and conformational destabilization energy terms for putative inhibitors. Using this modified scoring function, we have been able to identify 15 submicromolar-level IKK β inhibitors that possess the phenyl-(4-phenyl-pyrimidin-2-yl)-amine moiety as the molecular core. Decomposition analysis of the calculated binding free energies showed that a high biochemical potency could be achieved by lowering the desolvation cost and the conformational destabilization for the inhibitor required for binding to IKK β as well as by strengthening the interactions in the ATP-binding site. The formation of two hydrogen bonds with backbone amide groups of Cys99 in the hinge region was found to be necessary for tight binding of the inhibitors in the ATP-binding site. From molecular dynamics simulations of IKK β -inhibitor complexes, we also found that complete dynamic stability of the bidentate hydrogen bond with Cys99 was required for low nanomolar-level inhibitory activity. This implies that the scoring function for virtual screening and *de novo* design would be further optimized by introducing an additional energy term to measure the dynamic stability of the key interactions in enzyme–inhibitor complexes.



■ INTRODUCTION

Nuclear factor kappa-B (NF- κ B) protein is a ubiquitously expressed transcription factor and known to be a key regulator of immune responses, cell proliferation, cell death, and inflammation.^{1,2} In normal cells, NF- κ B is maintained in an inactive state in the cytoplasm through binding to inhibitor of kappa-B (I κ B) anchoring protein. However, when cells are stimulated by a variety of factors such as interleukin-1, tumor necrosis factor, lipopolysaccharide, hormone, and other signals, I κ B is phosphorylated by the I κ B kinase (IKK) complex, which results in I κ B degradation and NF- κ B activation. Ultimately, NF- κ B proteins released from I κ B translocate freely into the nucleus and induce the transcription of genes responsible for inflammation and cell survival. For this reason, NF- κ B has been regarded as a crucial mediator associated with a number of human cancers and inflammatory diseases. Several approaches to suppress NF- κ B activation are now being investigated. For example, a number of therapeutic agents including IKK inhibitors, proteasome inhibitors, and steroidal and non-steroidal anti-inflammatory drugs are known to mediate the blockade of the NF- κ B signaling pathway.³ The inhibition of IKK can thus be a promising strategy for developing therapeutics for diseases caused by aberrant NF- κ B activation.

The multisubunit IKK complex consists of two catalytic subunits (IKK α and IKK β) and an essential regulatory subunit NEMO (IKK γ).⁴ It is generally agreed that IKK β plays a more critical role than IKK α in activating the NF- κ B pathway because the former has even higher kinase activity than the latter.^{5,6} Therefore, the inhibition of IKK β has received considerable attention as an effective strategy for the treatment of inflammation-related diseases such as asthma, rheumatoid arthritis, and cancer.^{7–9}

A number of small molecules have been reported through intensive studies and drug discovery programs for the development of potent and selective IKK β inhibitors.^{10–20} In addition to various ATP competitive inhibitors, the allosteric inhibitors have also been shown to selectively impair the activity of IKK β .²¹ Although most IKK β inhibitors were identified via the high-throughput screening of a chemical library and the structural modifications of known inhibitors, some rational drug design approaches have also been actively pursued based on a variety of computational methods.^{22–25} However, the lack of 3D structure of IKK β has limited the applicability of the computational methods due to the

Received: October 16, 2014

Published: December 16, 2014

considerable uncertainty in estimating the biochemical potencies of putative inhibitors. Recently, X-ray crystal structures of IKK β have been reported both in the resting form and in complex with a potent inhibitor.^{26,27} Such structural information about the interactions between IKK β and small-molecule ligands can greatly aid in the design of more effective IKK β inhibitors.

The present study was undertaken to identify new potent IKK β inhibitors by consecutively applying the virtual screening of a large chemical library to find a lead compound and *de novo* design to optimize the inhibitory activity of the lead by chemical modifications. The newly identified IKK β inhibitors have potential to reveal anticancer activities because the impairment of IKK β activity leads to the perturbation of the inflammatory process required for cancer development. Besides the discovery of potent IKK β inhibitors, therefore, we also investigated the presence of their anticancer activities with respect to the pancreatic cancer cells.

Even when using a 3D structure of the target protein, virtual screening and *de novo* design have not always been successful due to the imperfections in the scoring function for the estimation of the binding free energy between the target protein and a putative ligand.^{28,29} One of the reasons for this inaccuracy lies in the neglect of ligand solvation effects, which leads to the overestimation of the binding affinity of a ligand with many polar groups.³⁰ Therefore, to enhance the efficiency of virtual screening and *de novo* design, we modified the existing scoring function by adding a proper molecular solvation free energy function. The addition of this new energy term reflects the desolvation cost for a ligand to be bound in the ATP-binding site of IKK β .

Furthermore, most popular docking and *de novo* design programs concentrate on finding the conformation of a ligand that can be bound most tightly in the binding pocket of the receptor. Although there might be a large energy difference between this bioactive conformation of a ligand and its minimum-energy structure,³¹ the conformational destabilization of the ligand is neglected or roughly approximated from molecular mechanics in most scoring functions. It is therefore apparent that the inaccuracy of the scoring function can be attributed, at least in part, to the improper description of the ligand conformation energy. Therefore, to further enhance the possibility of finding the potent inhibitors via *de novo* design, we calculated the ligand conformational energy term in the scoring function with *ab initio* quantum chemical calculations. We thus anticipated that the present virtual screening and *de novo* design procedures would enrich the chemical library with molecules that have a good inhibitory activity against IKK β . Finally, we also addressed the dynamical features required for highly potent IKK β inhibitors based on molecular dynamics (MD) simulations of the IKK β –inhibitor complexes. The results obtained in these comprehensive computational and experimental studies are expected to provide useful information for the discovery of new potent IKK β inhibitors.

MATERIALS AND METHODS

Virtual Screening of IKK β Inhibitors with Docking Simulations. We used the automated AutoDock program^{32,33} to calculate the binding mode and binding free energy of each molecule in the docking library. The procedure for constructing this docking library is detailed in Supporting Information. To improve the accuracy of virtual screening, the original AutoDock scoring function was modified to include a solvation free energy term for the ligand. The introduction of this additional energy term seemed to guarantee better prediction of

the ligand binding affinity by accounting for the effects of ligand solvation on the protein–ligand association. The modified scoring function to calculate the protein–ligand binding free energy in solution (ΔG_b^{aq}) can be expressed as follows.

$$\begin{aligned} \Delta G_b^{\text{aq}} = & W_{\text{vdW}} \sum_{i=1} \sum_{j=1} \left(\frac{A_{ij}}{r_{ij}^{12}} - \frac{B_{ij}}{r_{ij}^6} \right) \\ & + W_{\text{Hbond}} \sum_{i=1} \sum_{j=1} E(t) \left(\frac{C_{ij}}{r_{ij}^{12}} - \frac{D_{ij}}{r_{ij}^{10}} \right) + W_{\text{elec}} \sum_{i=1} \sum_{j=1} \frac{q_i q_j}{\epsilon(r_{ij}) r_{ij}} \\ & + W_{\text{tor}} N_{\text{tor}} + W_{\text{sol}} \sum_{i=1} S_i (O_i^{\text{max}} - \sum_{j \neq i} V_j e^{-r_{ij}^2/2\sigma^2}) \end{aligned} \quad (1)$$

The weighting factors for van der Waals interactions, hydrogen bonds, electrostatic interactions, and the entropic penalty, and the molecular solvation free energy term, were represented by W_{vdW} , W_{Hbond} , W_{elec} , W_{tor} , and W_{sol} , respectively. The interatomic distance is r_{ij} , and A_{ij} , B_{ij} , C_{ij} , and D_{ij} are Leonard-Jones potential parameters. The hydrogen-bond energy term includes an additional weighting factor, $E(t)$, to reflect the angle-dependent directionality. In calculating the electrostatic interaction energy term, we used the sigmoidal function $\epsilon(r_{ij})$ as the distance-dependent dielectric constant of IKK β .³⁴ In the torsional term, N_{tor} denotes the number of rotatable bonds in the ligand. The final term in eq 1 represents the desolvation cost of the ligand for binding to IKK β and includes three atomic parameters, S_i , O_i^{max} , and V_i , which denote the atomic solvation free energy per unit volume, maximum atomic occupancy, and fragmental volume for atom i , respectively.³⁵ This desolvation term was calculated using the atomic parameters reported by Park because they proved to be successful in estimating the hydration energies of various organic molecules.³⁶ Using this modified scoring function, we carried out docking simulations in the ATP-binding pocket of IKK β to score and rank the potential IKK β inhibitors according to the calculated binding affinities.

***De novo* Design.** The structure-guided *de novo* design of IKK β inhibitors was performed in three steps. First, we made some structural modifications to the initial IKK β inhibitor found from the preceding virtual screening to obtain the best scaffold from which even more potent inhibitors could be derivatized. The LigBuilder program³⁷ was used in this structural transformation to obtain phenyl-(4-phenylpyrimidin-2-yl)-amine (PPA) as a promising scaffold for designing new potent inhibitors. In the second step, a variety of PPA derivatives were generated based on the calculated binding mode of PPA in the ATP-binding site of IKK β . To obtain various PPA derivatives as candidates for a potent inhibitor, a genetic algorithm was employed to generate the derivatives by changing the chemical moieties at the substitution positions. In this step, we used the empirical scoring function suggested by Wang et al.³⁸ to score and rank the generated PPA derivatives. Because the central pyrimidin-2-yl amine group of PPA appeared to be bound tightly to the ATP-binding site, we limited the substitution positions to the two terminal phenyl rings. To reduce the computational time, only the generated derivatives that could satisfy the bioavailability rules as a drug candidate were selected for further analysis. Based on the filtration criteria, we obtained 3617 PPA derivatives that were estimated to have higher inhibitory activity against IKK β than PPA itself.

In the final *de novo* design step, the generated PPA derivatives were further screened with the new scoring function constructed by introducing a conformational destabilization energy term of ligand into the modified scoring function shown in eq 1. This new scoring function has the following form.

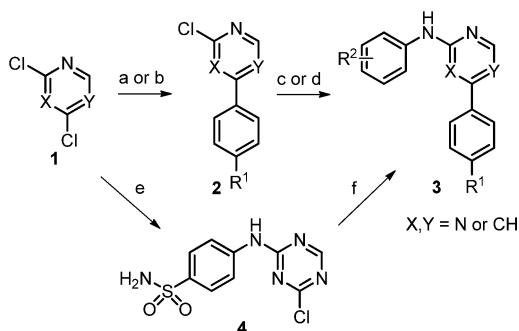
$$\Delta G_b^{\text{conf}} = \Delta G_b^{\text{aq}} + \Delta E_{\text{conf}} \quad (2)$$

Here, ΔE_{conf} represents the energy required for the conformational change of a ligand from its ground state to the best binding mode in the ATP-binding site of IKK β . This new energy term was augmented to the scoring function to enhance the accuracy of predicting the binding free energy of a ligand and could be given by the electronic

energy difference between the fully optimized structure of the ligand and its best binding conformation with respect to IKK β . We calculated this conformational destabilization energy with *ab initio* calculations at B3LYP/3-21G* level of theory. The PPA derivatives selected from the precedent *de novo* design were then rescored according to the binding affinities for IKK β calculated from additional docking simulations with the improved scoring function (ΔG_b^{conf}) in eq 2. Finally, the 100 top-ranked derivatives were inspected for the possibility of chemical synthesis.

Synthesis of PPA Derivatives. As illustrated in Scheme 1, the designed derivatives could be conveniently prepared by a two-step

Scheme 1. Preparation of Aminopyrimidine or Triazine Derivatives^a



^aReagents and conditions: (a) PdCl₂(PPh₃)₂, arylboronic acid, K₃PO₄, 1,4-dioxane/H₂O, 50 or 70 °C, 4–12 h; (b) Pd(PPh₃)₄, 2 N Na₂CO₃, MeCN, 90 °C, 3 h; (c) aniline, cat. HCl, EtOH, 150 °C, 30 min, microwave; (d) aniline, DMF, 80 °C, 30 min, then 1 N HCl, 80 °C, 4 h; (e) *p*-aminobenzenesulfonamide, DMF, 0 °C, 3 h; (f) Pd(dppf)Cl₂·CH₂Cl₂, arylboronic acid, K₃PO₄, 1,4-dioxane/H₂O, 140 °C, 1 h, microwave.

sequence: (1) aryl groups were installed at the 4-position of the pyrimidine core via palladium-catalyzed cross-coupling reactions with corresponding arylboronic acids; next, (2) the chloro compounds **1** were substituted with appropriate anilines by an S_NAr reaction to allow for the direct facile conversion to the product **2**. In the case of the triazine scaffold, a 4-sulfonamide aniline group was introduced at the triazine ring prior to Suzuki coupling to afford the target compounds.

Enzyme Assays. The inhibitory activities of all compounds with respect to IKK β were measured by Reaction Biology Corp. (Malvern, PA, USA) by means of radiometric kinase assays ([γ -³³P]-ATP). The enzymatic activity of IKK β was monitored using 20 μ M of IKKtide substrate dissolved in the freshly prepared Reaction Buffer (20 mM HEPES (pH 7.5), 10 mM MgCl₂, 1 mM EGTA, 0.02% BRIJ-35, 0.02 mg/mL BSA, 0.1 mM Na₃VO₄, 2 mM DTT, 1% DMSO). Each putative IKK β inhibitor was dissolved in 100% DMSO at the specific concentration and diluted in serial manner with epMotion 5070 in DMSO. Four nM of IKK β /IKKBK (Invitrogen) was added into the reaction buffer including 20 μ M of IKKtide substrate. After delivering the candidate inhibitor dissolved in DMSO into the kinase reaction mixture by Acoustic technology (Echo550; nanoliter range), the reaction mixture was incubated for 20 min at room temperature. To initiate the enzymatic reaction, ³³P-ATP with specific activity of 10 μ Ci/ μ L was delivered into the reaction mixture to reach the final ATP concentration of 1 μ M. Radioactivity was then monitored by the filter-binding method after the incubation of reaction mixture for 2 h at room temperature. At given concentrations of the inhibitor, biochemical potency was measured by the percent remaining kinase activity with respect to vehicle (dimethyl sulfoxide) reaction. Curve fits and IC₅₀ values were then obtained using the PRISM program (GraphPad Software). The ATP-competitive inhibitor staurosporine (STSP) was employed as the positive control in this study because of its high biochemical potency against various kinases including IKK β .³⁹

RESULTS AND DISCUSSION

Virtual Screening and Enzyme Assays. Of the 260,000 compounds in the docking library screened for tight binding in the ATP-binding site of IKK β , the 100 top-ranked compounds were selected as virtual hits. All these compounds were tested for the presence of inhibitory activity against IKK β at a concentration of 50 μ M by a high-throughput binding assay. Five compounds revealed significant biochemical potency with percent of control (POC) values lower than 30, and these were selected for the determination of the IC₅₀ values. The synthetic intermediates to obtain the candidate compounds for IKK β inhibitors were also screened for biochemical potency with respect to IKK β . However, no significant activity was observed at the concentration of 50 μ M. The chemical structures and inhibitory activities of the newly found IKK β inhibitors are presented in Figure 1. As the common structural features,

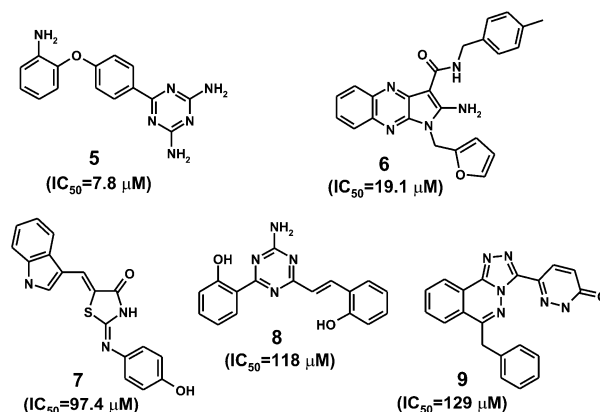


Figure 1. Chemical structures and IC₅₀ values of five IKK β inhibitors identified through the virtual screening of a chemical library with molecular docking.

compounds **5–9** possess several hydrogen-bonding groups and nonpolar aromatic rings. Hence, they seem to be capable of establishing multiple hydrogen bonds and hydrophobic contacts in the ATP-binding site of IKK β .

To address the inhibitory mechanisms of the newly identified IKK β inhibitors, we compared their binding modes calculated with the modified AutoDock scoring function (eq 1). The lowest-energy conformations of **5–9** are overlaid in Figure 2a in the ATP-binding site of IKK β . All five inhibitors appear to be stabilized in the unique binding pocket comprising the Gly loop (residues 20–30), the hinge region (residues 95–100) of the ATP-binding site, and the activation loop (residues 166–194) at the interface of the N- (residues 1–109) and C-terminal (residues 110–307) domains. It is a common feature in the calculated binding modes for all five inhibitors that they involve multiple hydrogen bonds and van der Waals contacts with the residues in the hinge region and those at the top of the C lobe, respectively. The binding modes of **5–9** are also similar in that some nonpolar moieties are directed to the Gly loop, which would act as a receptor with respect to the phosphate group in ATP binding. Therefore, the formation of hydrogen bonds with the hinge region and hydrophobic interactions with the Gly loop seem to contribute to the inhibition of IKK β by the effective blocking of ATP binding in a cooperative fashion. As a check on the possibility of the allosteric inhibition of IKK β by **5–9**, we conducted additional docking simulations with extended 3D grid maps to include the whole kinase domain.

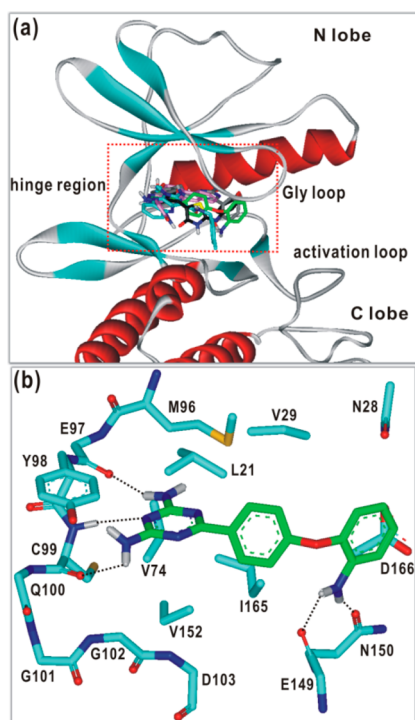


Figure 2. (a) Comparison of the docking poses for 5–9 in the ATP-binding site of IKK β . The carbon atoms of 5–9 are indicated in green, cyan, black, gray, and pink, respectively. (b) Detailed binding mode of 5 in the ATP-binding site of IKK β . The carbon atoms of 5 and IKK β are shown in green and cyan, respectively. Hydrogen bonds are indicated with dotted lines.

However, no peripheral binding pocket was found in which 5–9 could be stabilized with a negative binding free energy. It is thus expected that the inhibitory activity of 5–9 stems from specific binding in the ATP binding site of IKK β .

Because 5 is a small molecule with a molecular weight of 294.3 and has inhibitory activity at the micromolar level, detailed analysis of its binding mode would be helpful for designing new inhibitors with increased potency. Figure 2b illustrates the lowest-energy binding mode of 5. We note that the [1,3,5]triazine-2,4-diamine group of 5 donates two hydrogen bonds to the backbone aminocarbonyl oxygens of Glu97 and Cys99 and acts as a hydrogen-bond receptor with respect to the backbone amidic nitrogen of Cys99. These three hydrogen bonds seem to play a critical role in the inhibition of IKK β by 5, as the establishment of multiple hydrogen bonds with the backbone amide groups in the hinge region was found to be necessary for the binding of the inhibitor in the ATP-binding site of IKK β .²⁷ In the calculated IKK β -5 complex, two additional hydrogen bonds are established at the top of the C lobe between the terminal aniline moiety of 5 and the aminocarbonyl oxygens of Glu149 (backbone) and Asn150 (side chain). These two hydrogen bonds also seem to serve as a significant binding force to accommodate 5 in the ATP-binding site. Further stabilization of 5 in the binding pocket appears to be achieved through the hydrophobic interactions of its aromatic rings with the nonpolar side chains of Leu21, Val29, Val74, Tyr98, Val152, and Ile165. Judging from the features of the calculated binding mode of 5, the low micromolar inhibitory activity can be attributed to the simultaneous establishments of van der Waals contacts and multiple hydrogen bonds in the ATP-binding site of IKK β .

Energetic Features of the Identified Inhibitors. To investigate the effect of adding a ligand solvation term to the scoring function on the accuracy of the calculated binding affinities for IKK β , we carried out a decomposition analysis of the calculated binding free energies of 5–9. Because the binding free energy for the protein–ligand complex in solution (ΔG_b^{aq}) can be given by subtracting the ligand solvation free energy (ΔG^{sol}) from that in the gas phase (ΔG_b^{gas}), we computed the two energy terms separately to estimate their relative contributions to ΔG^{aq} . Table 1 lists ΔG_b^{gas} and ΔG_b^{aq}

Table 1. Binding Free Energies in the Gas Phase (ΔG_b^{gas}) and in Solution (ΔG_b^{aq}), Solvation Free Energy (ΔG^{sol}), and Conformational Destabilization Energy (ΔE^{conf}) for the IKK β Inhibitors 5–9^a

compd	ΔG_b^{gas}	ΔG^{sol}	ΔG_b^{aq}	ΔE^{conf}	ΔG_b^{conf}	$\Delta G_b^{\text{exp}b}$
5	−24.3	−12.7	−11.6	3.0	−8.6	−7.0
6	−26.8	−14.5	−12.3	5.6	−6.7	−6.4
7	−23.9	−13.3	−10.6	4.7	−5.9	−5.5
8	−24.3	−13.8	−10.5	4.1	−6.4	−5.4
9	−22.5	−11.2	−11.3	6.6	−4.7	−5.3

^aEach energy value is given in kcal/mol. ^bThe experimental ΔG_b (ΔG_b^{exp}) values were obtained from the corresponding K_i values calculated using the Cheng–Prusoff equation [$K_i = IC_{50}/(1 + [ATP]/K_m)$].

values for the five inhibitors in comparison to the corresponding ΔG^{sol} and the experimental ΔG_b (ΔG_b^{exp}) values. The calculated binding free energies of 5–9 are in better agreement with the experimental results due to the change of the original scoring function (ΔG_b^{gas}) to a more physically reasonable one (ΔG_b^{aq}) that includes the ligand desolvation term ($-\Delta G^{\text{sol}}$). For example, the ΔG_b^{gas} value of 5 appears to be higher than that of 6 by 2.5 kcal/mol and similar to those of 7 and 8, in conflict with its biochemical potency against IKK β being highest. On the other hand, 5 is found to have higher ΔG^{sol} value than 6–8, which implies a lower desolvation cost for binding in the ATP-binding site of IKK β . Thus, 5 can only be identified as a potent IKK β inhibitor using a scoring function that takes into account the desolvation cost for a ligand to form the required protein–ligand complex as well as the strength of interactions in the ATP-binding site. This result exemplifies the need to include the ligand solvation free energy term in the scoring function for successful virtual screening.

Despite the significant improvement, 6 is still predicted to be a more potent inhibitor than 5 according to the ΔG_b^{aq} values in contrast to the experimental results. Furthermore, the ΔG_b^{aq} value of 9 appears to be similar to that of 5, which is inconsistent with the more than 10-fold lower potency of the former (Figure 1). These discrepancies imply the necessity for further modification of the scoring function.

Recognizing the possibility that the conformational energy change of an inhibitor upon binding to the target protein (ΔE^{conf}) would have a significant influence on the binding affinity of an enzyme–inhibitor complex,^{40,41} we examined the effect of including the quantum mechanically calculated conformational destabilization energy on the accuracy of the scoring function for the virtual screening of IKK β inhibitors. Listed in the fifth column of Table 1 are the ΔE^{conf} values of 5–9 associated with the conformational change from their fully optimized geometries to the docked poses in the ATP-binding site of IKK β . These ΔE^{conf} values, calculated at B3LYP/3-21G*

level of theory, are small in magnitude as compared to the ΔG^{sol} and $\Delta G_{\text{b}}^{\text{gas}}$ values. This is not surprising because the molecular electronic energy is essentially calculated based on variational methods. Nonetheless, the introduction of the ΔE^{conf} term into the scoring function improves the accuracy in estimating the ligand binding affinity to a significant extent. When $\Delta G_{\text{b}}^{\text{exp}}$ values were compared to those of $\Delta G_{\text{b}}^{\text{aq}}$ plus ΔE^{conf} ($\Delta G_{\text{b}}^{\text{conf}}$), for example, it follows immediately that the binding affinities of **6** and **9** with respect to IKK β can fall below that of **5** due to the higher conformational destabilization upon binding in the ATP-binding site. Related to the accuracy enhancement by adding the ΔE^{conf} term, the root-mean-square (RMS) error with respect to the $\Delta G_{\text{b}}^{\text{exp}}$ values of **5–9** decreases (from 5.35 to 0.95 kcal/mol) when the scoring function changes from $\Delta G_{\text{b}}^{\text{aq}}$ to $\Delta G_{\text{b}}^{\text{conf}}$. Overall, the squared Pearson correlation coefficient (R^2) between the experimental and computational binding free energies of **5–9** increases from 0.31 to 0.76 due to the modifications of the scoring function by the addition of ΔG^{sol} and ΔE^{conf} terms. This indicates that the scoring function becomes even more powerful when the effects of ligand solvation and conformational destabilization are taken into account simultaneously.

De novo Design for the Change of the Inhibitor Scaffold. Although **5–9** are newly identified IKK β inhibitors and expected to have satisfactory physicochemical properties for drug candidates, they are poor lead compounds for drug discovery due to the low biochemical potencies. Therefore, we decided to make some structural modifications to the identified inhibitors to find more potent IKK β inhibitors with at least submicromolar-level inhibitory activity. Because **5–9** were actually selected from a chemical library of commercially available compounds that had been synthesized for a different purpose rather than as IKK β inhibitors, it would be reasonable to change their structural skeletons to design the new potent IKK β inhibitors. For this reason, we started with the structure-based *de novo* design of new IKK β inhibitors from the design of the new inhibitor scaffolds by modifying the 2-(4-phenoxyphenyl)-[1,3,5]triazine (**10**) moiety contained in **5**.

Two major criteria were applied to generate the new inhibitor scaffolds with *de novo* design. First, we selected only the structures similar to **10** with a Tanimoto coefficient higher than 7.0 because **10** proved to be well-accommodated in the ATP binding site (Figure 2). The output structures were screened further for having the lower $\Delta G_{\text{b}}^{\text{aq}}$ values than that of **10** to select a good inhibitor scaffold with an increased binding affinity for IKK β .

As a consequence of this multistep *de novo* design, we were able to find three structures (**11–13**) that were anticipated to be promising scaffolds from which new potent IKK β inhibitors could be derivatized. The structures and calculated binding free energies of **11–13** are shown in Figure 3 and Table 2, respectively, in comparison with those of **10**. As can be expected from the use of a similarity criterion in the *de novo* design, **11–13** are structurally similar with three six-membered

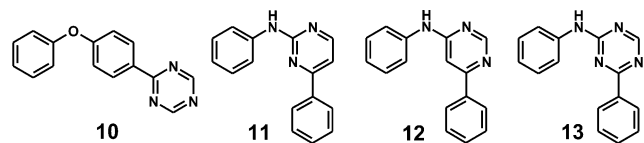


Figure 3. Structures of the inhibitor scaffolds (**11–13**) identified with *de novo* design using **10** as the input structure.

Table 2. Calculated $\Delta G_{\text{b}}^{\text{gas}}$, ΔG^{sol} , and $\Delta G_{\text{b}}^{\text{aq}}$ Values of the Newly Designed Inhibitor Scaffolds (**11–13**) in Comparison with Those of the Input Scaffold (**10**)^a

scaffold	10	11	12	13
$\Delta G_{\text{b}}^{\text{gas}}$	−15.9	−17.1	−16.7	−16.9
ΔG^{sol}	−6.8	−5.5	−6.4	−7.2
$\Delta G_{\text{b}}^{\text{aq}}$	−9.1	−11.6	−10.3	−9.7

^aEach energy value is given in kcal/mol.

aromatic rings. **11–13** seem to be the better inhibitor scaffolds than **10**, because the former are predicted to bind in the ATP-binding site of IKK β more tightly than the latter. Using **11–13** as the input structures, we carried out the second structure-based *de novo* design to find new potent IKK β inhibitors. To increase the accuracy, we used $\Delta G_{\text{b}}^{\text{conf}}$ in eq 2 as the scoring function to estimate the biochemical potencies of the generated derivatives of **11–13** considering the desolvation cost and the conformational destabilization associated with binding to IKK β .

To address the possibility of tight binding of the newly designed IKK β inhibitor scaffolds in the ATP-binding site, we compared their binding modes. Figure 4 shows the binding

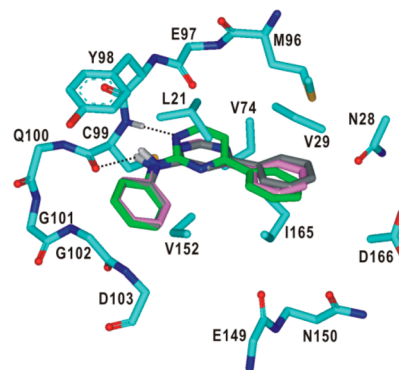


Figure 4. Calculated binding modes of **11–13** in the ATP-binding site of IKK β . The carbon atoms of IKK β , **11**, **12**, and **13** are indicated in cyan, green, gray, and pink, respectively. Hydrogen bonds are indicated with dotted lines.

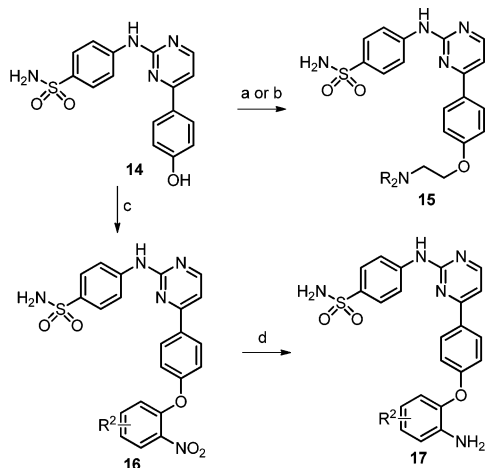
modes of **11–13** calculated with the modified AutoDock scoring function. All three putative inhibitor scaffolds appear to be in close contact with the hinge region through the two hydrogen bonds with the backbone groups of Cys99 in the bidentate form. This result is consistent with the X-ray crystallographic study on the IKK β -inhibitor complex, in which double hydrogen bonds with the backbone amide groups of the hinge region were found to be necessary for the effective inhibition of IKK β .²⁷ It is also a common feature in the calculated binding modes of **11–13** that three aromatic rings are stabilized through the hydrophobic interactions with the nonpolar residues in the Gly loop (Leu21 and Val29) and those at the top of C lobe (Val152 and Ile165). Because the *para* positions of the two terminal phenyl rings of **11–13** are farthest from the protein atoms, many potent IKK β inhibitors seem to be identified by introducing various chemical moieties at the two positions.

Structures and Potencies of the Designed and Synthesized IKK β Inhibitors. The PPA moiety might not be a new scaffold in the field of kinase inhibitors in the strict sense because it contains the amino pyrimidine group that has been considered as a useful structural element of kinase

inhibitors. However, many kinase inhibitors derivatized from the amino pyrimidine core were shown to have too poor physicochemical properties for cellular activity and bioavailability.^{42–44} In this study, therefore, we aimed to find the new PPA-based IKK β inhibitors with novel side chains through the simultaneous optimization of biochemical potency and drug-like properties in the structure-based *de novo* design. As a consequence of this design effort, we were able to synthesize the PPA derivatives as novel IKK β inhibitors that were expected to have better physicochemical properties and biochemical potencies than the known ones with the amino pyrimidine moiety.

Synthesis of compounds bearing modifications on the phenol group was carried out by Mitsunobu or S_N2 reactions to provide the linked analogues **15**. In addition, phenol intermediate **14** was reacted with substituted 1-fluoro-2-nitrobenzene to undergo nucleophilic aromatic substitution to produce the desired nitro derivatives **16**, which were further reduced under Fe/NH₄Cl conditions to afford amino derivatives **17**.

Scheme 2. Synthesis of Elaborated Aminopyrimidine Derivatives^a



^aReagents and conditions: (a) 2-(dimethylamino)-ethyl chloride·HCl, KI, K₂CO₃, DMF, 90 °C, 2 h, then 1.25 M HCl in MeOH, rt, 30 min; (b) *N*-Boc-ethanolamine, PPh₃, DIAD, THF, rt, 48 h, then 1.25 M HCl in MeOH, 50 °C, 1 h; (c) substituted 1-fluoro-2-nitrobenzene, K₂CO₃, DMSO, 130 °C, 2 h; (d) Fe, NH₄Cl, EtOH/H₂O, 85 °C, 30 min.

Table 3 lists the structures and IC₅₀ values of various derivatives of **11–13** that were selected for synthesis among the virtual hits of *de novo* design. Of the 25 derivatives synthesized and tested, 15 compounds reveal submicromolar-level inhibitory activities against IKK β . This high hit rate exemplifies the accuracy of the modified scoring function (ΔG_b^{conf} in eq 2) with which the new inhibitors can be designed to maximize the binding affinity for IKK β and simultaneously minimize the desolvation cost and the conformational destabilization associated with binding in the ATP-binding site of IKK β . As a check on the novelty of the synthesized IKK β inhibitors, we examined the availability of structural and functional data for all 24 synthesized compounds in the two popular chemical databases, SciFinder and PubChem. Compounds **19–42** were found to be completely new substances. Although **18** proved to be one of synthetic examples of the patent (US2006/

0079543A1), no structural and biological data have been reported so far. Hence, **18–42** are the first reported compounds as IKK β inhibitor.

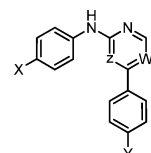
In Table 3, it should be noted that the majority of designed inhibitors include the sulfonamide moiety on the terminal phenyl ring connected to the central heterocyclic structure with the –NH– linker (X position). Because the terminal phenyl ring is most likely to reside between the hinge region and Gly loop (Figures 2 and 4) that play a critical role in ATP binding, the introduced sulfonamide group seems to serve as an effective surrogate for the phosphate group of ATP. The introduction of a sulfonamide group at the X position allows the high inhibitory activity against IKK β to be maintained for a variety of substituents at the *para* position of the terminal phenyl ring at the opposite side of the PPA core (Y position), which is evidenced by the submicromolar inhibitory activities of **18**, **24–27**, **33–39**, **41**, and **42**. The necessity of a terminal sulfonamide moiety for high biochemical potency becomes more apparent when the IC₅₀ value of **27** is compared to those of **28–32**, which indicates that change or removal of the sulfonamide group leads to a 30–150-fold decrease in the inhibitory activity. Thus, a derivative of **11** with a sulfonamide moiety at the X position can be suggested as a good lead compound for drug discovery with IKK β as the target protein.

Whereas the replacement of chloride at Y position in **18** with intact and fluorinated phenoxy groups in **21–24** lowers the biochemical potency by 10–100 times, some highly potent inhibitors with IC₅₀ values of 60–80 nM can be obtained upon the substitution of 2-aminoethoxy group (**25** and **26**) at Y position. Judging from the IC₅₀ values of **35–39** lower than those of **33** and **34** by 1 order of magnitude, the nitrophenoxy moiety seems to be the better substituent than the amino-phenoxy moiety in terms of conferring high inhibitory activity against IKK β . A potent IKK β inhibitor (**41**) with a similar IC₅₀ value to those of **35–39** can also be obtained by simply substituting the –NH₂ group at the Y position. It is also noteworthy that the biochemical potency decreases to the micromolar level in going from **35** to **40** due to the methyl substitution at the terminal sulfonamide group, which confirms its crucial role as a structural element of potent IKK β inhibitors.

Among the variety of substituents at the Y position studied, the sulfonamide moiety in **42** is found to be most efficient for the inhibition of IKK β . As a consequence of the substitutions of two sulfonamide moieties at the X and Y positions of the PPA core, the highly potent IKK β inhibitor **42** is identified, with an IC₅₀ value of 4 nM. Because the terminal phenyl ring that includes the Y position is expected to reside at the top of the C lobe (Figure 4), the sulfonamide group at the Y position seems to be stabilized through hydrogen bonds with the polar groups at the interface between the Gly loop and the C lobe.

Consistent with the ΔG_b^{aq} value of **11** being lower than those of **12** and **13**, which is mainly due to the decrease in the desolvation cost (Table 2), the inhibitory activity of **18** is found to be even higher than those of **19** and **20** by more than 3 orders of magnitude. This result is surprising due to the high degree of similarity among the molecular structures of **18–20**. Such an unexpectedly large difference in the IC₅₀ values actually indicates the involvement of an additional factor beyond the desolvation effect in the variation of inhibitory activities with respect to the structural perturbation in the central aromatic heterocycle.

To investigate the biological activities of the IKK β inhibitors found in this study, we carried out the cell-based assays for the

Table 3. Structures and Inhibitory Activities of the Derivatives of 11–13 against IKK β ^a


Compd	X ^a	Y ^a	Z	W	IC ₅₀ (nM)	Compd	X ^a	Y ^a	Z	W	IC ₅₀ (nM)
18		Cl	N	C	19	31	H-		N	C	11800
19		Cl	C	N	30600	32	MeO-		N	C	12000
20		Cl	N	N	27200	33			N	C	322
21			N	C	1524	34			N	C	922
22			N	C	973	35			N	C	34
23			N	C	1220	36			N	C	45
24			N	C	233	37			N	C	21
25			N	C	79	38			N	C	30
26			N	C	65	39			N	C	32
27			N	C	98	40			N	C	1125
28			N	C	2730	41		H ₂ N-	N	C	41
29			N	C	14200	42			N	C	4
30			N	C	8180	STSP					28

^aAsterisk indicates the atom bonded to substitution position.

26, 35, 41, and 42 using the pancreatic cancer cell lines (BxPC-3). In this study, cell viability was measured at varying concentrations of the inhibitors with 3-(4,5-dimethylthiazol-2-yl)-2,5-diphenyltetrazolium bromide method. All four compounds appear to have significant inhibitory activity against the proliferation of the pancreatic cancer cell lines in a dose-dependent manner with IC₅₀ values ranging from 3 to 10 μ M (Table 4). These apparent antiproliferative activities of 26, 35,

Table 4. IC₅₀ Values with Respect to the Inhibition of BxPC-3 Cell Proliferation by IKK β Inhibitors

	26	35	41	42
IC ₅₀ (μ M)	6.2	9.6	3.7	8.5

41, and 42 with respect to BxPC-3 cancer cell line imply that they can serve as a starting point for the discovery of new anticancer medicines. However, we note that the biochemical potencies decrease from nanomolar level in enzyme inhibition assays to micromolar level in cell-based assays. As widely discussed in the literature,^{45–47} the relatively low anticellular activity of highly potent enzyme inhibitors can be attributed in a large part to the poor cell permeability. Therefore, further structural modifications to improve the cellular permeability seem to be necessary for the IKK β inhibitors found in this

study to become a good lead compound for the discovery of new cancer medicines.

As a check on the promiscuous inhibition of various kinases by the IKK β inhibitors identified in this study, we investigated the selectivity profiles of the two representative compounds (26 and 35) via high-throughput target screening assay (KINOMEscan, Ambit Biosciences). The inhibitory activities of 26 and 35 were measured by POC values at the concentration of 10 μ M over a panel of 50 cancer-related kinases. The results for the measurements of these off-target activities are presented in Table S1. Consistent with the nanomolar inhibitory activities for IKK β , both compounds appear to bind tightly at the ATP-binding site of IKK β with zero POC value. Aside from the two IKK isoforms, only glycogen synthase kinase 3 beta (GSK3 β) and vascular endothelial growth factor receptor 2 (VEGFR2) are found to be adequate for effective binding of 26 with the associated POC values lower than 20. Similarly, 35 reveals a significant off-target binding affinity only for stem cell factor receptor (c-KIT), polo-like kinase 3 (PLK3), and MAP/microtubule affinity-regulating kinase 3 (MARK3) with the POC values of 9.5, 20, and 21, respectively. Such a preference of binding for a few kinases supports the possibility that the impairment of kinase activity of IKK β by the inhibitors found in

this study would stem from the specific binding in the ATP-binding site rather than compound promiscuity.

We next focus our attention on the energetic features associated with the stabilization of the newly identified IKK β inhibitors in the ATP-binding site. Table 5 lists the calculated

Table 5. Calculated ΔG_b^{gas} , ΔG^{sol} , ΔG_b^{aq} , ΔE^{conf} , and ΔG_b^{conf} values (in kcal/mol) for the IKK β Inhibitors in Comparison to the Corresponding ΔG_b^{exp} Values Calculated Using the Cheng–Prusoff Equation

compd	ΔG_b^{gas}	ΔG^{sol}	ΔG_b^{aq}	ΔE^{conf}	ΔG_b^{conf}	ΔG_b^{exp}
18	-22.0	-11.2	-10.8	1.7	-9.1	-10.5
19	-22.4	-12.5	-9.9	3.7	-6.2	-6.1
20	-21.5	-13.4	-8.1	2.3	-5.8	-6.2
21	-25.3	-13.6	-11.7	4.6	-7.1	-7.9
22	-26.0	-13.8	-12.2	5.4	-6.8	-8.2
23	-25.5	-14.1	-11.4	4.5	-6.9	-8.1
24	-25.2	-14.6	-10.6	4.2	-6.4	-9.0
25	-25.0	-12.9	-12.1	4.0	-8.1	-9.7
26	-25.1	-13.3	-11.8	4.7	-7.1	-9.8
27	-27.0	-15.4	-11.6	3.2	-8.4	-9.6
28	-26.7	-13.6	-13.1	5.3	-7.8	-7.6
29	-25.5	-15.0	-10.5	5.6	-4.9	-6.6
30	-23.8	-12.5	-11.3	5.9	-5.4	-6.9
31	-23.2	-11.2	-12.0	5.6	-6.4	-6.7
32	-24.8	-11.8	-13.0	6.3	-6.7	-6.7
33	-27.6	-16.2	-11.4	4.1	-7.3	-8.8
34	-26.3	-15.3	-11.0	3.4	-7.6	-8.2
35	-27.1	-14.7	-12.4	4.6	-7.8	-10.2
36	-27.9	-14.4	-13.5	4.3	-9.2	-10.0
37	-28.7	-15.4	-13.3	4.8	-8.5	-10.5
38	-28.2	-15.1	-13.1	3.7	-9.4	-10.3
39	-28.4	-14.9	-13.5	3.9	-9.6	-10.2
40	-26.7	-13.8	-12.9	6.1	-6.8	-8.1
41	-24.1	-13.3	-10.8	1.9	-8.9	-10.1
42	-27.8	-16.6	-11.2	1.8	-9.4	-11.4
STSP	-26.6	-14.8	-11.8	2.2	-9.6	-10.3

ΔG_b^{gas} , ΔG_b^{aq} , ΔG^{sol} , ΔE^{conf} , and ΔG_b^{conf} values for 18–42 in comparison to the corresponding ΔG_b^{exp} values. The standard deviations of ΔG_b^{gas} , ΔG^{sol} , and ΔE^{conf} values among 25 inhibitors amount to 2.0, 1.4, and 1.3 kcal/mol, respectively. This similarity indicates that these three energy components contribute to ΔG_b^{conf} to a comparable extent and confirms that both the desolvation cost for a ligand and its conformational destabilization upon binding to IKK β should be considered important energy terms in the scoring function for virtual screening and *de novo* design of potent IKK β inhibitors. Therefore, to increase the biochemical potency of an IKK β inhibitor with structural modifications, the resultant strengthening of enzyme–inhibitor interactions should be sufficient to surmount the combined potency-lowering effects that stem from the increased stabilization in solution and the increased conformational destabilization at the ATP-binding site.

Comparison of the ΔG_b^{gas} , ΔG_b^{aq} , ΔG_b^{conf} , and ΔG_b^{exp} values of 18 with those of 19 and 20 clearly reveals that the much lower inhibitory activities of the latter can be attributed to the combined effect of the increases in the desolvation cost and conformational instability. Within the framework of the solvation model inherent in the fifth term in eq 1, 18 should be less stable in solution than 19 because it is difficult to completely expose one of the aromatic nitrogens to the bulk

solvent due to the screening effects of the neighboring phenyl and –NH– groups. In addition to such a reduced desolvation cost, the 2-aminopyrimidine core in 18 can also achieve the cis conformation with respect to the C–NH bond without a significant loss of conformational stability because there is little steric repulsion between the central pyrimidine and the neighboring phenyl ring, which facilitates the establishment of a stable bidentate hydrogen bond with the backbone groups of Cys99. This is actually not the case for 4-aminopyrimidine core in 19 because the exchange of the nitrogen and –CH– group at the Z and W positions (Table 3) would force the two aromatic rings out of planarity to avoid a poor van der Waals contact between the hydrogen at the Z position and the neighboring phenyl ring. The weakening of the biochemical potency with the change of the scaffold from 2- to 4-aminopyrimidine was also observed in SAR studies for the inhibitors of Bcr-Abl kinase.⁴⁸ In case of 20, the low biochemical potency can be attributed in large part to the increase in the desolvation cost for binding to IKK β due to the change of the central aromatic ring from pyrimidine to triazine, which is implied in the 2.2 kcal/mol decrease of the ΔG^{sol} value in going from 18 to 20.

The importance of the contribution from the conformational destabilization for a ligand to the binding free energy can become more apparent by comparing the ΔG_b^{aq} and ΔE^{conf} values of potent inhibitors, such as 41 and 42, to those of inhibitors with moderate strength including 21, 28, and 40. Although the average ΔG_b^{aq} value of the former is 1.6 kcal/mol higher than that of the latter, a decrease of more than 2.7 kcal/mol in the conformational destabilization for binding in the ATP-binding site makes the ΔG_b^{conf} values of the former lower than those of the latter, which is consistent with the experimental results.

The high inhibitory activities of 35–39 are surprising because they are predicted to have a relatively high desolvation cost and to undergo significant conformational destabilization upon binding to IKK β (Table 5). However, as can be inferred from the highly negative ΔG_b^{gas} values, both potency-lowering effects can be successfully compensated by strengthening the interactions with the residues in the ATP-binding site. This indicates that one can also augment the potency of an IKK β inhibitor with structural modifications in such a way as to make the interactions with IKK β strong enough to surmount both the increased desolvation cost and the conformational destabilization upon binding in the ATP-binding site. Thus, the decomposition analyses of ΔG_b^{conf} provide energetic insight into the biochemical action of IKK β inhibitors.

Because all inhibitors possessing sulfonamide and nitrophenoxy groups at the X and Y positions (35–39), respectively, were shown to have high biochemical potency due to the low ΔG_b^{gas} values, we investigated their binding modes with docking simulations. As shown in Figure 5, both the sulfonamide and nitrophenoxy moieties of 35 and 38 appear to be in close contact with protein groups. More specifically, their nitrophenoxy group is well-accommodated in a small binding pocket comprising the side chains of Asn28, Lys44, Lys147, Glu149, Asn150, Ile165, and Asp166. Because most of these amino acid residues are hydrophilic, the terminal nitro group of 35–39 seems to be stabilized through the attractive electrostatic interactions. More remarkably, we see that the sulfonamide moiety of 35 and 38 establishes three hydrogen bonds around the ATP-binding site with the side-chain of Lys106 and the backbone amide groups of Leu21 and Asp103. This is why the

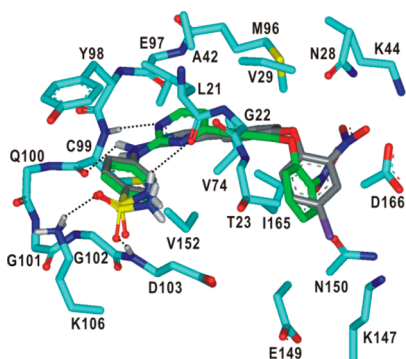


Figure 5. Calculated binding modes of **35** and **38** in the ATP-binding site of IKK β . The carbon atoms of IKK β , **35**, and **38** are indicated in cyan, green, and gray, respectively.

most potent IKK β inhibitors listed in Table 3 possess a sulfonamide moiety at the X position. The multiple hydrogen bonds involving the sulfonamide moiety are most likely to be critically important for the inhibition of IKK β because they involve the residues that belong to the hinge region (Asp103) and Gly loop (Leu21), which are the two key functional motifs for kinase action.

To investigate the effects of including the desolvation and conformational energy terms in the scoring function on the accuracy of the *de novo* design, we plotted the correlation diagrams between the experimental binding free energies and those calculated with the ΔG_b^{gas} and ΔG_b^{conf} functions. As observed in Figure 6a, we obtained an R^2 value of 0.316 for the comparison of ΔG_b^{exp} and ΔG_b^{gas} data for **18–42**, which indicates a very weak correlation between the experimental and calculated results. In contrast, the R^2 value increased to 0.759 after changing the variables from ΔG_b^{gas} and ΔG_b^{conf} (Figure 6b). This implies that the scoring function can become even more physically reasonable with the addition of the desolvation and

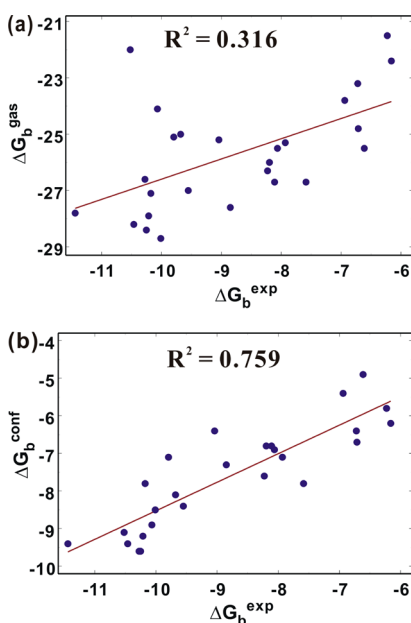


Figure 6. Correlation diagrams for the experimental binding free energies (ΔG_b^{exp}) of **18–42** and STSP versus those calculated with (a) ΔG_b^{gas} and (b) ΔG_b^{conf} including the desolvation and conformational destabilization energy terms for a ligand.

conformational destabilization energy terms for the ligand. The RMS error of the binding free energies of **18–42** estimated with ΔG_b^{conf} with respect to the experimental values is only 1.43 kcal/mol, compared to 17.0 kcal/mol in the absence of the two additional terms. This improvement is consistent with the results for **5–9** (Table 1). These substantial enhancements in both correlation and precision confirm the necessity for including the desolvation and the conformational destabilization energy of ligand in calculating the protein–ligand binding affinity.

Despite the substantial accuracy improvement due to the two additional energy terms, the scoring function ΔG_b^{conf} remains inadequate for fully elucidating the relative potencies of **18–42**. For example, the predicted binding free energies of **18**, **24**, **26**, and **35** become worse with the addition of the conformational destabilization energy term to ΔG_b^{aq} to obtain ΔG_b^{conf} . Furthermore, when the ΔG_b^{conf} and ΔG_b^{exp} values are compared, it follows immediately that the binding affinities of **24**, **26**, **35**, **37**, and **42** are underestimated by more than 2 kcal/mol.

Dynamic Stabilities of the Hydrogen Bonds between the Pyrimidin-2-lyamine Group and Cys99. Because the bidentate hydrogen bond between the backbone groups of Cys99 and the central pyrimidin-2-lyamine moiety appears to be necessary for the tight binding of potent IKK β inhibitors, their relative biochemical potencies may be elucidated on the basis of the stabilities of the two hydrogen bonds. To examine the effects of dynamic properties of the bidentate hydrogen bond on the inhibitory activity, we carried out 10.2 ns MD simulations of the IKK β -**18**, IKK β -**38**, and IKK β -**42** complexes in aqueous solution. These three enzyme–inhibitor complexes were selected in the comparative MD studies to find the characteristic dynamic properties of the bidentate hydrogen bond for **42** with low nanomolar inhibitory activity that could be discriminated from those for the inhibitors with IC₅₀ values ranging from 10 to 50 nM such as **18** and **38** (Table 3). This comparative study seems to be necessary to obtain insight into designing nanomolar IKK β inhibitors because the ΔG_b^{conf} scoring function is incapable of distinguishing the inhibitory activity of **42** from those of **18** and **38** (Table 5).

Figure 7 shows the time evolutions of the interatomic distances to measure the stabilities of the bidentate hydrogen bonds between Cys99 and the central pyrimidin-2-ylamine moiety of the inhibitor in IKK β -**18**, IKK β -**38**, and IKK β -**42** complexes. We note that the N–H \cdots N hydrogen bond between amidic nitrogen of Cys99 and the central pyrimidine ring becomes dynamically more stable with the change of the inhibitor from **18** and **38** to **42** (Figure 7a). For example, it appears to be retained for 99.6% of simulation time in IKK β -**42** complex when the distance limit for a hydrogen bond is assumed to be 2.5 Å,⁴⁹ as compared to 88.4% and 82.6% of residence time in IKK β -**18** and IKK β -**38** complexes, respectively. Similarly, the O \cdots H–N hydrogen bond between the aminocarbonyl oxygen of Cys99 and the pyrimidin-2-ylamine moiety of the inhibitors is observed in 99.8% of the trajectory snapshots of IKK β -**42** complex, whereas it is preserved for 96.3% and 97.9% of simulation time in IKK β -**18** and IKK β -**38** complexes (Figure 7b), respectively. It is thus apparent that the bidentate hydrogen bond between Cys99 and the inhibitor in IKK β -**42** complex should be dynamically more stable than those in the IKK β -**18** and IKK β -**38** complexes. Therefore, the higher biochemical potency of **42** than **18** and **38** can be attributed, at least in part, to the strengthening of the bidentate hydrogen bonds with Cys99 in the ATP-binding site.

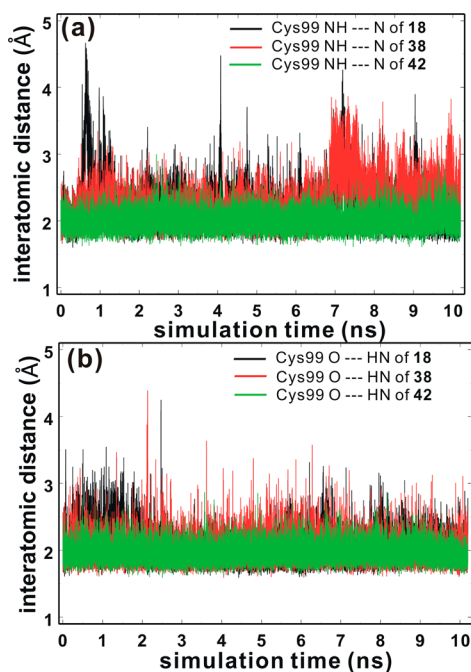


Figure 7. Time evolutions of the interatomic distances associated with (a) N–H···N and (b) O···H–N hydrogen bonds established between the backbone amide groups of Cys99 and the central pyrimidin-2-ylamine moiety of 18, 38, and 42.

This result exemplifies the need to consider the detailed dynamical aspects of enzyme–inhibitor interactions to precisely estimate the inhibitory activity of the highly potent inhibitors.

Because 42 possesses two sulfonamide moieties at both X and Y positions in the PPA core, they are expected to contribute significantly to the high dynamic stability of the bidentate hydrogen bonds in the IKK β -42 complex. Figure 8

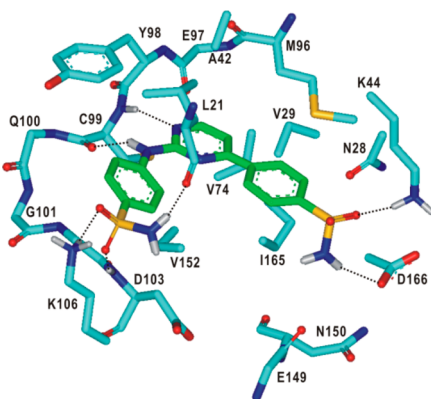


Figure 8. A representative MD trajectory snapshot of IKK β -42 complex. The carbon atoms of IKK β and 42 are indicated in cyan and green, respectively. Hydrogen bonds are indicated with dotted lines. Solvent molecules are omitted for clarity.

displays a representative MD trajectory snapshot for the IKK β -42 complex. The interactions of 42 in the ATP-binding site of IKK β are similar to those of 35 and 38 (Figure 5) in that the sulfonamide group at the X position forms three hydrogen bonds with the side chain of Lys106 and the backbone groups of Leu21 and Asp103 at the interface between the hinge region and the Gly loop. The second sulfonamide moiety at the Y position also establishes multiple hydrogen bonds with the side

chains of Lys44 and Asp166, respectively, at the interface between the N and C lobes. These hydrogen bonds seem to be strong because they involve a charged group. The formation of five additional hydrogen bonds by the two sulfonamide groups is expected to have an effect of supporting the bidentate hydrogen bonds between Cys99 and 42 by preventing the dissociation of the inhibitor from the ATP-binding site. The high inhibitory activity of 42 may thus be elucidated in terms of the stability of the bidentate hydrogen bond with Cys99.

The highly negative $\Delta G_{\text{B}}^{\text{gas}}$ value of 42 (Table 5) actually stems from the formation of a total of seven stable hydrogen bonds in the ATP-binding site of IKK β . However, these multiple hydrogen bonds may be insufficient to compensate for the high desolvation cost for binding to IKK β (Table 5) due to the presence of two highly polar sulfonamide groups. 42 can thus be a nanomolar-level inhibitor by successfully overcoming the high desolvation cost with the two additional potency-enhancing factors including the low conformational destabilization upon binding in the ATP-binding site and the increased dynamic stability of the bidentate hydrogen bonds with Cys99.

CONCLUSIONS

We have identified new potent IKK β inhibitors by means of the structure-based virtual screening of a large chemical library and subsequent *de novo* design using the PPA as the molecular core. To improve the efficiency of this computer-aided drug design, we improved the scoring function by introducing proper desolvation energy and conformational destabilization energy terms for ligands. As a consequence of these modifications, the discovery of new IKK β inhibitors was successful to the extent that more than the half of the designed PPA derivatives had submicromolar inhibitory activities. In particular, the derivative with sulfonamide moieties on both terminal phenyl rings (42) was anticipated to serve as a good lead compound for the discovery of new small-molecule medicines because of its low nanomolar-level inhibitory activity. We found that the biochemical potency could be optimized by lowering the desolvation cost and the conformational destabilization for the inhibitor required for binding to IKK β as well as by reinforcing the interactions in the ATP-binding site. Consistent with the previous experimental findings, the establishment of the hydrogen bonds with the backbone amide groups of Cys99 in the hinge region proved to be indispensable for high inhibitory activity against IKK β . The MD simulation studies of IKK β -inhibitor complexes showed that the dynamic stabilities of the bidentate hydrogen bonds between Cys99 and the inhibitor would serve as the yardstick for discriminating the submicromolar and low nanomolar IKK β inhibitors. Therefore, to identify the highly potent IKK β inhibitors with virtual screening and *de novo* design, the scoring function should include the energy term to measure the dynamic stability of the bidentate hydrogen bonds with Cys99 in addition to those to describe the strength of interactions in the ATP-binding site, the ligand desolvation cost, and the conformational destabilization of the inhibitor upon binding to IKK β .

ASSOCIATED CONTENT

Supporting Information

Computational details, experimental procedures, selectivity profiles of 26 and 35 with respect to kinase inhibitions, characterization data, and copies of ^1H and ^{13}C NMR spectra for all compounds. This material is available free of charge via the Internet at <http://pubs.acs.org>.

AUTHOR INFORMATION

Corresponding Authors

hspark@sejong.ac.kr

hongorg@kaist.ac.kr

Notes

The authors declare no competing financial interest.

ACKNOWLEDGMENTS

This research was supported by National Research Foundation of Korea (NRF) funded by the Ministry of Education, Science and Technology (NRF-2011-0022858) and the Institute for Basic Science (IBS-R010-G1).

REFERENCES

- (1) Nakanishi, C.; Toi, M. *Nat. Rev. Cancer* **2005**, *5*, 297.
- (2) Perkins, N. D. *Nat. Rev. Mol. Cell Biol.* **2007**, *8*, 49.
- (3) Karin, M.; Yamamoto, Y.; Wang, Q. M. *Nat. Rev. Drug Discovery* **2004**, *3*, 17.
- (4) Yamamoto, Y.; Gaynor, R. B. *Trends Biochem. Sci.* **2004**, *29*, 72.
- (5) Li, J.; Peet, G. W.; Pullen, S. S.; Schembri-King, J.; Warren, T. C.; Marcu, K. B.; Kehry, M. R.; Barton, R.; Jakes, S. *J. Biol. Chem.* **1998**, *273*, 30736.
- (6) Hu, Y.; Baud, V.; Delhase, M.; Zhang, P.; Deerinck, T.; Ellisman, M.; Johnson, R.; Karin, M. *Science* **1999**, *284*, 316.
- (7) Bamborough, P.; Callahan, J. F.; Christopher, J. A.; Kerns, J. K.; Liddle, J.; Miller, D. D.; Morse, M. A.; Rumsey, W. L.; Williamson, R. *Curr. Top. Med. Chem.* **2009**, *9*, 623.
- (8) Suzuki, J.; Ogawa, M.; Muto, S.; Itai, A.; Isobe, M.; Hirata, Y.; Nagai, R. *Expert Opin. Investig. Drugs* **2011**, *20*, 395.
- (9) Colotta, F.; Allavena, P.; Sica, A.; Garlanda, C.; Mantovan, A. *Carcinogenesis* **2009**, *30*, 1073.
- (10) Liddle, J.; Bamborough, P.; Barker, M. D.; Campos, S.; Chung, C. W.; Cousins, R. P.; Faulder, P.; Heathcote, M. L.; Hobbs, H.; Holmes, D. S.; Ioannou, C.; Ramirez-Molina, C.; Morse, M. A.; Osborn, R.; Payne, J. J.; Pritchard, J. M.; Rumsey, W. L.; Tape, D. T.; Vicentini, G.; Whitworth, C.; Williamson, R. A. *Bioorg. Med. Chem. Lett.* **2012**, *22*, 5222.
- (11) Christopher, J. A.; Bamborough, P.; Alder, C.; Campbell, A.; Cutler, G. J.; Down, K.; Hamadi, A. M.; Jolly, A. M.; Kerns, J. K.; Lucas, F. S.; Mellor, G. W.; Miller, D. D.; Morse, M. A.; Pancholi, K. D.; Rumsey, W.; Solanke, Y. E.; Williamson, R. *J. Med. Chem.* **2009**, *52*, 1098.
- (12) Qiu, X.; Du, Y.; Lou, B.; Zuo, Y.; Shao, W.; Huo, Y.; Huang, J.; Yu, Y.; Zhou, B.; Du, J.; Fu, H.; Bu, X. *J. Med. Chem.* **2010**, *53*, 8260.
- (13) Lorenzo, P.; Alvarez, R.; Ortiz, M. A.; Alvarez, S.; Piedrafita, F. J.; de Lera, A. R. *J. Med. Chem.* **2008**, *51*, 5431.
- (14) Crombie, A. L.; Sum, F. W.; Powell, D. W.; Hopper, D. W.; Torres, N.; Berger, D. M.; Zhang, Y.; Gavriil, M.; Sadler, T. M.; Arndt, K. *Bioorg. Med. Chem. Lett.* **2010**, *20*, 3821.
- (15) Bingham, A. H.; Davenport, R. J.; Fosbeary, R.; Gowers, L.; Knight, R. L.; Lowe, C.; Owen, D. A.; Parry, D. M.; Pitt, W. R. *Bioorg. Med. Chem. Lett.* **2008**, *18*, 3622.
- (16) Waelchli, R.; Bollbuck, B.; Bruns, C.; Buhl, T.; Eder, J.; Feifel, R.; Hersperger, R.; Janser, P.; Revesz, L.; Zerwes, H. G.; Schlapbach, A. *Bioorg. Med. Chem. Lett.* **2006**, *16*, 108.
- (17) Palanki, M. S. S.; Erdman, P. E.; Ren, M.; Suto, M.; Bennett, B. L.; Manning, A.; Ransone, L.; Spooner, C.; Desai, S.; Ow, A.; Totsuka, R.; Tsao, P.; Toriumi, W. *Bioorg. Med. Chem. Lett.* **2003**, *13*, 4077.
- (18) Kishore, N.; Sommers, C.; Mathialagan, S.; Guzova, J.; Yao, M.; Hauser, S.; Huynh, K.; Bonar, S.; Mielke, C.; Albee, L.; Weier, R.; Graneto, M.; Hanau, C.; Perry, T.; Tripp, C. S. *J. Biol. Chem.* **2003**, *278*, 32861.
- (19) Ziegelbauer, K.; Gantner, F.; Lukacs, N. W.; Berlin, A.; Fuchikami, K.; Niki, T.; Sakai, K.; Inbe, H.; Takeshita, K.; Ishimori, M.; Komura, H.; Murata, T.; Lowinger, T.; Bacon, K. B. *Br. J. Pharmacol.* **2005**, *145*, 178.
- (20) Frelin, C.; Imbert, V.; Griessinger, E.; Loubat, A.; Dreano, M.; Peyron, J. F. *Oncogene* **2003**, *22*, 8187.
- (21) Burke, J. R.; Pattoli, M. A.; Gregor, K. R.; Brassil, P. J.; MacMaster, J. F.; McIntyre, K. W.; Yang, X.; Iotzova, V. S.; Clarke, W.; Strnad, J.; Qiu, Y.; Zusi, F. C. *J. Biol. Chem.* **2003**, *278*, 1450.
- (22) Hu, H.; Snyder, J. P. *J. Chem. Inf. Model.* **2012**, *52*, 3190.
- (23) Lauria, A.; Ippolito, M.; Fazzari, M.; Tutone, M.; Blasi, F. D.; Mingoia, F.; Almerico, A. M. *J. Mol. Graph. Model.* **2010**, *29*, 72.
- (24) Noha, S. M.; Atanasov, A. G.; Schuster, D.; Markt, P.; Fakhruddin, N.; Heiss, E. H.; Schrammel, O.; Rollinger, J. M.; Stuppner, H.; Dirsch, V. M.; Wolber, G. *Bioorg. Med. Chem. Lett.* **2011**, *21*, 577.
- (25) Nagarajan, S.; Choo, H.; Cho, Y. S.; Oh, K. S.; Lee, B. H.; Shin, K. J.; Pae, A. N. *Bioorg. Med. Chem.* **2010**, *18*, 3951.
- (26) Xu, G.; Lo, Y.-C.; Li, Q.; Napolitano, G.; Wu, X.; Jiang, X.; Dreano, M.; Karin, M.; Wu, H. *Nature* **2011**, *472*, 325.
- (27) Liu, S.; Misquitta, Y. R.; Olland, A.; Johnson, M. A.; Kelleher, K. S.; Kriz, R.; Lin, L. L.; Stahl, M.; Mosyak, L. *J. Biol. Chem.* **2013**, *288*, 22758.
- (28) Huang, S. Y.; Grinter, S. Z.; Zou, X. *Phys. Chem. Chem. Phys.* **2010**, *12*, 12899.
- (29) Warren, G. L.; Andrews, C. W.; Capelli, A. M.; Clarke, B.; LaLonde, J.; Lambert, M. H.; Lindvall, M.; Nevins, N.; Semus, S. F.; Senger, S.; Tedesco, G.; Wall, I. D.; Woolven, J. M.; Peishoff, C. E.; Head, M. S. *J. Med. Chem.* **2006**, *49*, 5912.
- (30) Shoichet, B. K.; Leach, A. R.; Kuntz, I. D. *Proteins* **1999**, *34*, 4.
- (31) Viji, S. N.; Prasad, P. A.; Gautham, N. *J. Chem. Inf. Model.* **2009**, *49*, 2687.
- (32) Morris, G. M.; Goodsell, D. S.; Halliday, R. S.; Huey, R.; Hart, W. E.; Belew, R. K.; Olson, A. J. *J. Comput. Chem.* **1998**, *19*, 1639.
- (33) Park, H.; Lee, J.; Lee, S. *Proteins* **2006**, *65*, 549.
- (34) Mehler, E. L.; Solmajer, T. *Protein Eng.* **1991**, *4*, 903.
- (35) Stouten, P. F. W.; Frömmel, C.; Nakamura, H.; Sander, C. *Mol. Simul.* **1993**, *10*, 97.
- (36) Park, H. *J. Comput.-Aided Mol. Des.* **2014**, *28*, 175.
- (37) Wang, R.; Gao, Y.; Lai, L. *J. Mol. Model.* **2000**, *6*, 498.
- (38) Wang, R.; Liu, L.; Lai, L. *J. Mol. Model.* **1998**, *6*, 379.
- (39) Liu, T.; Zhan, W.; Wang, Y.; Zhang, L.; Yang, B.; Dong, X.; Hu, Y. *Eur. J. Med. Chem.* **2014**, *73*, 167.
- (40) Viji, S. N.; Prasad, P. A.; Gautham, N. *J. Chem. Inf. Model.* **2009**, *49*, 2687.
- (41) Kontoyianni, M.; McClellan, L. M.; Sokol, G. S. *J. Med. Chem.* **2004**, *47*, 558.
- (42) Palmer, W. S.; Alam, M.; Arzeno, H. B.; Chang, K.-C.; Dunn, J. P.; Goldstein, D. M.; Gong, L.; Goyal, B.; Hermann, J. C.; Hogg, J. H.; Hsieh, G.; Jahangir, A.; Janson, C.; Jin, S.; Kammlott, R. U.; Kuglstatter, A.; Lukacs, C.; Michoud, C.; Niu, L.; Reuter, D. C.; Shao, A.; Silva, T.; Trejo-Martin, T. A.; Stein, K.; Tan, Y.-C.; Tivitmahaisoon, P.; Tran, P.; Wagner, P.; Weller, P.; Wu, S.-Y. *Bioorg. Med. Chem. Lett.* **2013**, *23*, 1486.
- (43) Gong, L.; Han, X.; Silva, T.; Tan, Y.-C.; Goyal, B.; Tivitmahaisoon, P.; Trejo, A.; Palmer, W.; Hogg, H.; Jahagir, A.; Alam, M.; Wagner, P.; Stein, K.; Filonova, L.; Loe, B.; Makra, F.; Rotstein, D.; Raptova, L.; Dunn, J.; Zuo, F.; Porto, J. D.; Wong, B.; Jin, S.; Chang, A.; Tran, P.; Hsieh, G.; Niu, L.; Shao, A.; Reuter, D.; Hermann, J.; Kuglstatter, A.; Goldstein, D. *Bioorg. Med. Chem. Lett.* **2013**, *23*, 3565.
- (44) Deininger, M.; Buchdunger, E.; Druker, B. J. *Blood* **2005**, *105*, 2640.
- (45) Kerns, E. H.; Di, L. *Drug Discovery Today* **2003**, *8*, 316.
- (46) Innocenti, P.; Cheung, K.-M. J.; Solanki, S.; Mas-Droux, C.; Rowan, F.; Yeoh, S.; Boxall, K.; Westlake, M.; Pickard, L.; Hardy, T.; Baxter, J. E.; Aherne, G. W.; Bayliss, R.; Fry, A. M.; Hoelder, S. *J. Med. Chem.* **2012**, *55*, 3228.
- (47) Ginman, T.; Viklund, J.; Malmström, J.; Blid, J.; Emond, R.; Forsblom, R.; Johansson, A.; Kers, A.; Lake, F.; Sehgelmeble, F.; Sterky, K. J.; Bergh, M.; Lindgren, A.; Johansson, P.; Jeppsson, F.; Fälting, J.; Gravenfors, Y.; Rahm, F. *J. Med. Chem.* **2013**, *56*, 4181.

- (48) Deng, X.; Okram, B.; Ding, Q.; Zhang, J.; Choi, Y.; Adrián, F. J.; Wojciechowski, A.; Zhang, G.; Che, J.; Bursulaya, B.; Cowan-Jacob, S. W.; Rummel, G.; Sim, T.; Gray, N. S. *J. Med. Chem.* **2010**, *53*, 6934.
- (49) Jeffrey, G. A. *An Introduction to Hydrogen Bonding*; Oxford University Press: Oxford, 1997.